Regular ring dynamics in AX_2 tetrahedral glasses

R. A. Barrio
Instituto de Física, Universidad Nacional Autónoma de México, Apartado Postal 20-364, 01000 México, Distrito Federal, México

F. L. Galeener*
Department of Physics, Colorado State University, Fort Collins, Colorado 80523

E. Martínez†
Departamento de Física Fundamental, Universidad Autónoma de Madrid, CIII, Canto Blanco, Madrid, Spain

R. J. Elliott
Theoretical Physics, Department of Physics, University of Oxford, 1 Keble Road, Oxford OX1 3NP, United Kingdom
(Received 10 May 1993)

We review the experimental evidence and qualitative arguments for the existence of small highly regular rings of bonds in amorphous (a-)SiO_2 and selected other AX_2 tetrahedral glasses. The structure and vibrations of planar 3-rings and regular puckered 4-rings in a-SiO_2 are then modeled using Born central and noncentral forces. The vibrational coupling of these rings to the more disordered glass network is modeled by attaching a Bethe lattice at each connection. The calculated vibrational properties of the breathing modes of the rings are found to be quite consistent with the observed frequencies, linewidths, and isotope shifts of the sharp lines D_1 and D_2 seen in the Raman spectra of a-SiO_2. The results support the previous assignment of D_2 (606 cm^{-1}) to a planar 3-ring and D_1 (495 cm^{-1}) to a regular ring. Similar calculations for a-GeO_2 are consistent with the suggestion that this material contains a substantial concentration of nearly planar 3-rings. Our methods can be generalized to treat similar forms of intermediate range order in glasses having other network connectivities.

I. INTRODUCTION

Exact determination of the structure of an amorphous solid is impossible, owing primarily to the absence of global translational or rotational symmetries. Since chemical bonding imposes approximate rotational symmetry of nearest neighbors about a given species, it is best to attempt first to determine the structure on this shortest length scale, and then endeavor to discern additional order on increasingly larger scales of distance. This plan has led to a fairly precise delineation of four scales of distance,[1] termed *short, intermediate, long, and global.* The present paper presents calculational methods enabling the use of vibrational spectroscopy as a probe of glass structure on the *intermediate* scale of distance.

A. Ranges of order

Short-range order (SRO) describes the nearest-neighbor bonding environment of each atomic species. The elements of SRO in a-SiO_2 can be visualized with the help of Fig. 1 where one can see schematically the SRO around the Si (or A) atom and that around the O (or X) atom. Every atom of type A is surrounded approximately by a tetrahedron of X atoms and every X atom bridges between two A atoms. The relative position of two neighboring tetrahedra is determined by the intertetrahedral angle θ and the dihedral angle δ. Disorder in real glasses, such as SiO_2, is associated with variations in *both* angles, although the typical spread in δ is thought to be much larger than in θ.[2] In the "continuous random network" (CRN) model, δ is taken to be random and uncorrelated with position in the glass structure.[3]

In the present definition of SRO, all neighbors of

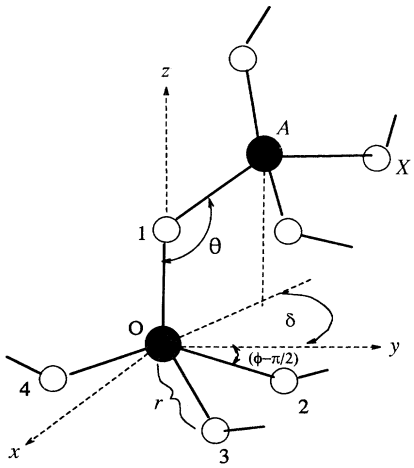

FIG. 1. The local geometry of a 4-2 connected tetrahedral AX_2 glass, such as a-SiO_2. The "intertetrahedral" angle is θ and the "dihedral" angle is δ. Short-range order (SRO) involves specification of the tetrahedral arrangement (r, θ) about X. Specification of δ is an element of intermediate-range order (IRO).

a species are treated as if they are *spherically symmetric*. This allows a logical separation of SRO from intermediate-range order (which recognizes that the neighbors and their associated environments are not spherically symmetric, and have orientations associated with them). It follows that θ is an element of SRO, but δ is not.

Intermediate-range order (IRO) involves specification of relative atomic positions over several nearest-neighbor distances, given the SRO. Most fundamentally, IRO recognizes that the nearest neighbors are not spherically symmetric. IRO may take the form of specification of δ, a distribution of δ, distributions of the sizes of completed rings of bonds ("ring statistics"), properties of network connectivity, etc.

Long-range order (LRO) allows for the possibility of translational repetition of an IRO over several repeat lengths and thus accounts for the possible existence of microcrystals in the structure of amorphous solids.

Global-range order (GRO) accounts for structural order defined over macroscopic (entire sample) distances, including specification of network connectivity, chemical order, isotropy, and the like.

Elsewhere, Galeener[4] has described several models for a-SiO_2 in terms of all their elements of SRO, IRO, LRO, and GRO. In this paper we will make very little further mention of LRO and GRO. We are in effect providing a correction to the Zachariasen-Warren CRN model,[3] by showing that in a-SiO_2 the dihedral angle δ is *not* randomly distributed, but at various places in the glass is spatially correlated so as to give small highly regular rings of Si-O bonds at those places.

B. Sharp lines D_1 and D_2 in the Raman spectra of vitreous SiO_2

The Raman spectra for parallel (HH) and perpendicular (HV) polarizations of vitreous (v-)SiO_2, reduced by the Bose-Einstein thermal population factor according to the prescription of Shucker and Gammon[5] and Galeener and Sen,[6] has been published earlier many times [see for instance Ref. 11 and Fig. 5(a) in this paper]. The HH spectrum consists mainly of broad features which peak at about 450 cm^{-1}, 800 cm^{-1}, 1065 cm^{-1}, and 1200 cm^{-1}. These have been identified[7–9] as "network" modes, accounted for by coupled vibrations of a CRN, assuming random dihedral angles δ. Thus, the broad features are accounted for by SRO only. The CRN model produces one high frequency mode, which is thought to be split into a TO-LO pair[10] at 1065 and 1200 cm^{-1}, respectively. The vibrations of this network and the shape of the HH Raman spectrum have been modeled quite well with a Bethe lattice, whose details are reported by Barrio, Galeener, and Martínez.[11,12]

The two sharp lines D_1 (495 cm^{-1}) and D_2 (606 cm^{-1}) cannot be explained by the same CRN–Bethe-lattice model.[12] D_1 and D_2 have full width at half maximum (FWHM) linewidths of 20 cm^{-1} and 30 cm^{-1}, respectively, and are highly polarized (HH$\gg$HV). Their strength and position in bulk v-SiO_2 have been studied variously as a function of neutron bombardment,[13,14] sample fictive temperature,[15–17] trace water content,[18–20] isotopic substitution on Si,[21] isotopic substitution on O,[22] tensile stress,[23] and pressure compaction.[24] These observations eliminate virtually all explanations in terms of wrong bonds or broken bonds.[25–27]

As a result, Galeener[28] was forced to consider regions of *increased* order, IRO in the form of highly regular rings of bonds, connected into the otherwise more disordered network at sites whose possible special nature is unknown. Because D_2 is stronger in porous Vycor glass[29] and in partially desiccated sol-gel glasses,[30] Galeener[31] has suggested that the D_2 structures are more numerous in the vicinity of the v-SiO_2 surface. These observations and suggestions have been expanded extensively by Brinker and co-workers.[32]

C. Mechanism for small rings to be regular

One of the striking features of D_1 and D_2 is their extreme narrowness, about an order of magnitude smaller than the 200 cm^{-1} width of the dominant broad Raman line (R) which peaks at ~450 cm^{-1}. The Bethe lattice fit to the width of the broad features of the Raman spectrum is consistent with a distribution of θ having FWHM of about 30°.[12]

From empirical selection rules[33] supported by a bond polarizability model[34] Galeener[35] has argued that highly polarized Raman lines in glasses must correspond to symmetric stretch (SS) motions of the kinds shown in Ref. 35. Since R, D_1, and D_2 are highly polarized and occur at similar frequencies, it is likely their motions are similar, namely, SS motions of the bridging oxygen atom along the bisector of θ.[35] This means that the θ for D_1 and D_2 must be much more tightly controlled than that for R. This necessary control is supplied by the regularity of the proposed rings, and regularity can be expected according to the following argument, given in more detail Ref. 28.

Figure 2 is an estimate of the energy of a Si-O-Si bridge as a function of the angle θ, based on theoretical calculations of Newton and Gibbs (NG).[36] The minimum angle $\langle\theta\rangle$ is ~150°, and this is close to the most probable value of θ in the glass, as revealed by x-ray diffraction.[37]

For a regular planar 3-ring, θ has the value $\theta_3 = 130.5°$, on the reasonable assumption that the O-Si-O angle is always closely tetrahedral (109.5°). If this ring is "puckered" or made nonplanar, each of its three Si-O-Si angles will be *less than or equal* to 130.5°. According to Fig. 2(a) puckered 3-ring will therefore have a higher total bridge energy than a planar one. Thus, when a 3-ring is formed in a glass melt, it will relax its three θ values towards minimum energy at $\theta = \theta_3$ for all three bridges. It will "unpucker" because there is a strong driving force for a 3-ring, once formed, to lose energy by becoming planar, and hence regular.

When the 3-ring has become planar, it can further reduce its energy only by breaking a bond and becoming part of a different ring with $n > 3$. This necessity for bond breaking provides a *kinetic* "bottleneck" at θ_3 (less than $\langle\theta\rangle$) and provides a rationale for the existence of significant concentration of highly regular planar 3-rings in v-SiO_2.

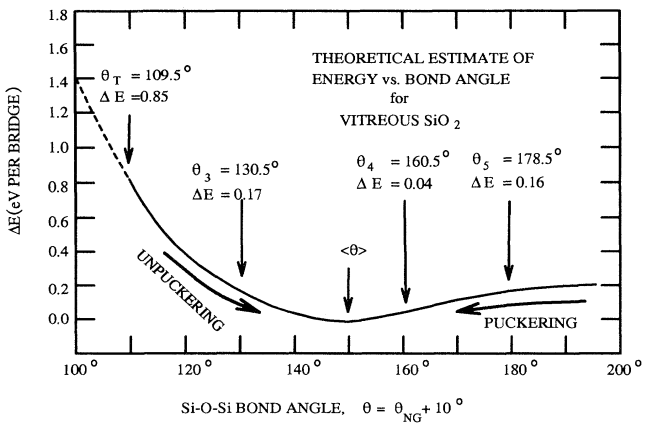

FIG. 2. Dependence of the energy of a ≡Si-O-Si≡ bridge on the -O- bridge angle θ, estimated using theoretical results of Ref. 36. This enables estimation of the energy of formation of various planar rings having the angles θ_n marked in the figure. The heavy arrows show the tendencies for minimization of energy by "puckering" and "unpuckering" of rings. It follows for *minimum* energy that 3-rings are planar and 4-rings are puckered with all $\theta = \langle\theta\rangle$.

On the other hand, Fig. 2 shows that θ_4 for a regular planar 4-ring is 160.5°, and is larger than $\langle\theta\rangle$. Thus a planar 4-ring, once formed, can reduce its energy by puckering so that some or all of its θ values are less than θ_4 and closer to $\langle\theta\rangle$. Since θ_4 is not far above $\langle\theta\rangle$, we assume that a significant number of 4-rings will relax to the lowest value $\langle\theta\rangle$. Those relaxed 4-rings which are (nearly) regular will exist in otherwise unexpectedly high concentration because they are at an *energetic* "bottleneck" of lowest possible energy. This provides a rationale for the existence of a significant concentration of regular puckered 4-rings in v-SiO_2.

Steric requirements of the network will not allow all rings with $n > 3$ to fall to lowest energy, and it therefore seems likely that the number of regular rings with $n = 5$, $n = 6$, etc., will be much less than those with $n = 4$. Thus we argue that the only significant concentrations of regular rings in v-SiO_2 have $n = 3$ (planar) or $n = 4$ (puckered). Moreover, these small-n regular rings are to be *expected* on grounds of energy minimization.

This method of predicting whether or not significant numbers of regular small-n rings are to be expected has been applied to eight rather different AX_2 tetrahedral glasses in Ref. 38. The number of anomalously sharp Raman lines (such as D_1 and D_2) thus predicted agrees with observation for all eight glasses.

D. Energetics of D_1 and D_2 in vitreous SiO_2

The previous discussion allows a crude estimate of the energy of formation of planar 3-rings (E_3) and regular puckered 4-rings (E_4). Galeener[35] assumed that these rings are formed on the average by taking the necessary n bridges from a "sea" of average bridges with $\theta = \langle\theta\rangle$. Using Fig. 2, the planar 3-ring requires 3 bridges, each with energy 0.17 eV, so that $E_3 \simeq 0.51$ eV. Similarly, the regular 4-ring requires 4 bridges, each with energy 0.04 eV, so that $E_4 \simeq 0.16$ eV. Subsequently, O'Keeffe and Gibbs[39] used first principles calculations to estimate E_3 and E_4, producing values close to experiment on D_1 and D_2.

The energies of formation of D_1 and D_2 have been measured by one of the authors and his co-workers,[15,17] as follows. A sample of v-SiO_2 was annealed at a high temperature T_F until a steady state structure was achieved. The sample was then quenched rapidly to room temperature and the areas under D_1 and D_2 were carefully measured. Those areas exhibit Arrhenius behavior versus inverse T_F as depicted in Fig. 3. The area under D_1 shows an energy of formation of 0.14 eV while D_2 shows 0.40 eV.

Comparison of these experimental energies of formation with the theoretical estimates of E_3 and E_4 gives strong reason to identify D_1 with the regular 4-ring and D_2 with the planar 3-ring. Assignment on this basis is especially important because it is independent of the uncertainties to be associated with the calculation of vibrational frequencies.

E. Vibrational decoupling of regular rings in an otherwise disordered network

Raman spectra of v-SiO_2 after isotopic substitution on the silicon atoms[21] and on the oxygen atoms[22] show definitively that the atomic motions for R, D_1, and D_2 [Fig. 5(a)] are essentially all oxygen motion, with no silicon motion involved.

Since D_1 and D_2 lie in the same frequency range as R, and all these lines are highly polarized (hence represent symmetric stretch of oxygen atoms), one could normally expect the motions of D_1 and D_2 to couple strongly with

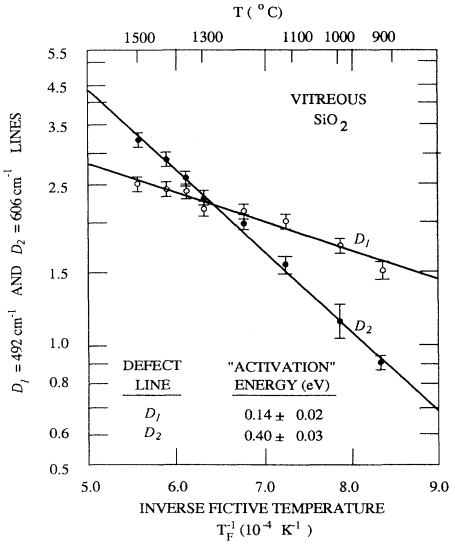

FIG. 3. Concentrations of the Raman active "defects" D_1 and D_2 versus the inverse fictive temperature T_F, showing Arrhenius behavior $\sim \exp(-\Delta E/kT_F)$ with energies of formation ΔE shown.

those of R. This poses a serious technical problem. If D_1 and D_2 are to be narrow band vibrational units, coupled into the more disordered network, then their frequencies will be broadened, and shifted, so as to give much broader features for D_1 and D_2 than are observed.

The quantitative resolution of this problem is a central theme of the present paper, aspects of which were previously reported by the present authors[40] (GBME). We argue here that the sharp lines are particular symmetric stretch motions of regular rings that are *fully* connected into the host network; these motions give sharp lines because the rings are regular structures, and because the particular motions are localized to the rings, hence do not couple to the similar motions of the host network. As we shall see, this occurs in a way that automatically also satisfies the isotopic substitution data. We shall repeat the argument of GBME for vibrational decoupling of the breathing mode of the planar 3-rings, as well as appropriate regular but nonplanar n-rings.

Consider first the planar 3-ring in Fig. 4. It is connected to the rest of the network by six Si-O bonds (four of them shown and labeled BL in Fig. 4). In general these oxygen atom (○) displacements will exert a force on the Si atoms, which will communicate their motion to the rest of the network by distorting the BL bonds: This will broaden the breathing-mode frequency by an amount that we shall calculate later, in Secs. II B 3 and II C 4. On the other hand, if there happens to be zero *net* force on the Si atoms, they will remain stationary, and the breathing O motion in the ring will *not* be coupled to the network. In the rest of this paper we demonstrate that D_1 and D_2 are consistent with the breathing modes of regular 4-rings and planar 3-rings, respectively, and that these modes are approximately decoupled from the rest of the network, in the manner just described.

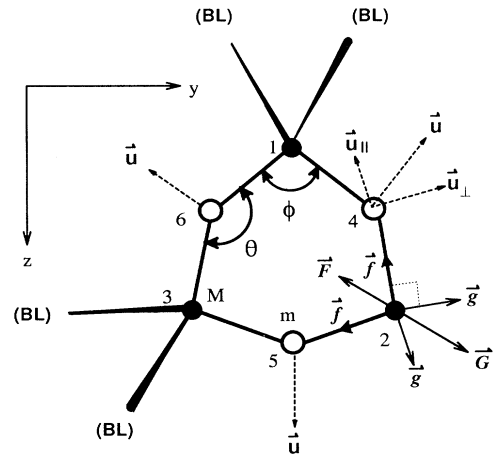

FIG. 4. The breathing mode of the planar 3-ring assigned to the sharp line D_2 in Fig. 1. When the net "central" force $\vec{F}$ on each Si atom (•) is canceled by the net "noncentral" force $\vec{G}$, the Si atoms are motionless, the mode is vibrationally decoupled from the rest of the network, and there is no isotope shift (for this mode). Approximate decoupling of this mode enables the 3-ring to explain all known properties of the D_2 line. In the calculations the atoms are numbered as shown and are all in the y-z plane. There are bonds labeled (BL) which are at angles $\phi_T/2$ with the plane and are connected to appropriately oriented Bethe lattices to represent the glass network in which the ring is embedded.

It is easy to derive a mathematical condition for such decoupling in terms of the Born force constants α and β, where α measures the "central" (or length restoring) force and β the "noncentral" (or bond orientation restoring) force. Other more complicated force constant models can be used,[41] but the Born forces are the simplest and most convenient and are known to be successful in modern work on the "optical" vibrations of networks representing disordered solids.[41] (Even so, it should be noted that the Born noncentral forces cannot correctly model all of the acoustic modes of a solid.[42])

The individual central ($\vec{f}$) and noncentral ($\vec{g}$) forces acting on a Si atom are shown in the lower right of Fig. 4. In the absence of Si motion, the magnitudes of these forces are given by $f = \alpha' u_{\parallel} = \alpha' u \cos(\theta/2)$ and $g = \beta' u \sin(\theta/2)$, where the u are defined in Fig. 4 and the prime denotes the force constant for a bond *within* the ring. The magnitudes of the oppositely directed total central ($\vec{F}$) and noncentral ($\vec{G}$) forces acting on the Si atom are then given by $F = 2f\cos(\phi/2)$ and $G = 2g\sin(\phi/2)$. The absence of Si motion requires $F = G$, so that perfect decoupling occurs when α'/β' has the value

$$(\alpha'/\beta')_d = \tan(\theta/2)\tan(\phi/2). \tag{1}$$

The frequency ω_d of the breathing mode at perfect decoupling follows simply from the fact that the Si atoms are at rest, so that only the oxygen atoms in this ring are in motion. Consider the oxygen atom executing breathing motion at the upper right in Fig. 4. The net force inward is $2f\cos(\theta/2) + 2g\sin(\theta/2)$. Application of Newton's second law to the oxygen mass m yields

$$\omega^2 = \frac{2\alpha'}{m}\cos^2(\theta/2) + \frac{2\beta'}{m}\sin^2(\theta/2)$$

or

$$\omega^2 = \left(\frac{\alpha'}{m}\right)\left[(1+\cos\theta) + \left(\frac{\beta'}{\alpha'}\right)_d (1-\cos\theta)\right], \tag{2}$$

where m is the mass of the O atom. In the case of the planar 3-ring, where $\theta = \theta_3 = 130.5°$, and using $\phi = \phi_T = \cos^{-1}(-1/3) \sim 109.5°$, one has

$$\left(\frac{\beta'}{\alpha'}\right)_d = 0.326 \tag{3}$$

and

$$\omega_d^2 = 0.888(\alpha'/m). \tag{4}$$

Note that Eqs. (1)–(4) involve ring parameters only: *Perfect decoupling of the breathing mode is a property of the regular ring, not of the vibrational systems to which*

it is attached. Note also that the perfect decoupling condition [Eq. (1)] is independent of the masses: It is a relationship between force constants and geometry alone.

Perfect decoupling by this mechanism requires that $\vec{F}$ and $\vec{G}$ be antiparallel at all Si atoms in the ring. This is possible for a regular 3-ring (where all θ are equal) only when the ring is planar. It may be verified that there are only three conformations of the 3-ring that can be regular (always assuming that $\phi \simeq 109.5°$): the planar, the "crown," and the "oxygen chair" conformations. The crown can be obtained by puckering the planar ring so that the three O atoms are left in the basal plane while the three Si atoms are tilted upward by a common amount forming a new plane parallel to and above the basal plane. The oxygen chair has three Si atoms in the basal plane, two O atoms tilted up, and one O atom tilted down as if the Si atoms formed the "seat" of a (shallow) chair, the O atoms its "back" and "legs." Similar conformations will be depicted explicitly for a 4-ring in Sec. II. It can also be readily verified that in the present two nonplanar cases, breathing motion along the bisector of θ produces $\vec{F}$ and $\vec{G}$ which *cannot* be antiparallel.

Equations (1) and (2) are also correct for perfect decoupling of oxygen breathing modes of any regular planar ring of order n; in those cases one evaluates the equations for $\phi = \phi_T = \cos^{-1}(-1/3) \simeq 109.5°$ and $\theta = \theta_n = 360(1 - n^{-1}) - \phi$ in degrees. The force resolutions at the Si atom are precisely as in Fig. 4 for the planar 3-ring, and so Eq. (1) follows exactly as before. At perfect decoupling, the force resolutions at the O atoms are also as before, and so Eq. (2) is verified for a planar n-ring.

Equations (1) and (2) are also correct for certain regular nonplanar conformations of some n-rings. These require that for oxygen breathing along the bisector of θ the $\vec{F}$ and $\vec{G}$ forces induced at the Si atom are antiparallel. In Sec. II C 1 we note that of the seven regular nonplanar conformations of a 4-ring, this antiparallel condition is satisfied only for the "oxygen boat." The oxygen boat 4-ring is therefore the only regular puckered 4-ring that is capable of perfect decoupling of its oxygen breathing mode, and obeys Eqs. (1) and (2) when decoupled.

It is this vibrational decoupling of the breathing mode of a regular n-ring that allows both for sharp Raman lines and for the absence of Si motion in the lines. We will illustrate the sharpness with detailed calculations in later sections.

For practical applications, one often desires ω^2 in units of wave numbers, $W(\mathrm{cm}^{-1})$. Expressions of the form $\omega^2 = k/M$ are then evaluated according to

$$W^2(\mathrm{cm}^{-2}) = 1.698 \times 10^4 \frac{\alpha(\mathrm{N/m})}{M(\mathrm{amu})}, \tag{5}$$

where α is expressed in newtons per meter and M in atomic mass units.

We reemphasize that the motional decoupling here is only for the *breathing* mode under the condition of Eq. (1). In general when Eq. (1) is satisfied other modes of the ring will be strongly coupled to the external systems represented by BL in Fig. 4.

II. CALCULATIONS BASED ON THE CLUSTER–BETHE-LATTICE APPROXIMATION

A. Dynamics of the continuous random network

In order to study the complete dynamics of a regular ring embedded in an amorphous network, one must model the elastic properties of both the ring and the amorphous network that is attached to the ring. In the cluster–Bethe-lattice approximation,[43] the geometry and force constants of the external network at each connection is modeled by identical Bethe lattices.[40,44] The Bethe lattice is mathematically convenient because it has no rings of bonds and its vibrational properties are especially tractable using a Born model Hamiltonian with both central and noncentral forces between nearest neighbors.

In an earlier paper Barrio, Galeener, and Martínez[12] (BGM) solved the Bethe lattice for an AX_2 tetrahedral glass on the assumption of Born force constants α and β, a single intertetrahedral angle θ everywhere, and a random distribution of the dihedral angle δ, in Fig. 1. Their results for the vibrational density of states and the Raman and infrared spectra of v-SiO_2 provided a best fit to the broad features of the experimental spectra when they used $\theta = 154°$, $\alpha = 507$ N/m, and $\beta = 78$ N/m. We shall use these parameters and their formalism to model the amorphous network at each place where it attaches to the regular ring of interest.

BGM used a Green's function formulation to study the vibrational density of states (VDOS) and the normal modes of the Bethe lattice for the CRN model of v-SiO_2. The derivation of the displacement-displacement Green's function was reported in detail, and so we shall merely restate essential results in order to apply their theory to the present problem.

In the Born Hamiltonian the potential between two nearest neighbor $(A - X)$ atoms is

$$V_{12} = \frac{\alpha - \beta}{2} \{(\vec{u}_1 - \vec{u}_2) \cdot \hat{\mathbf{e}}_{12}\}^2 + \frac{\beta}{2}(\vec{u}_1 - \vec{u}_2)^2, \tag{6}$$

where $\hat{\mathbf{e}}_{12}$ is a unit vector along the line joining atom 1 and atom 2, and α and β are the central and noncentral force constants, respectively. The interaction between a Si atom at the origin of coordinates and a nearest-neighbor oxygen along the z axis is then represented by

$$\mathbf{D}_1 = \begin{pmatrix} -\beta & 0 & 0 \\ 0 & -\beta & 0 \\ 0 & 0 & -\alpha \end{pmatrix}. \tag{7}$$

If, instead of a single oxygen atom, one attaches a whole SiO_2 Bethe lattice, one obtains a frequency dependent effective interaction

$$\langle \mathbf{K}_1 \rangle = \begin{pmatrix} -K_\perp & 0 & 0 \\ 0 & -K_\perp & 0 \\ 0 & 0 & -K_\parallel \end{pmatrix}. \tag{8}$$

This is diagonal as a result of taking a single θ everywhere and averaging over all (totally random) dihedral angles.

There is an exact solution for $\langle \mathbf{K}_i \rangle$ in BGM, showing that the Green's function at the tetrahedral Si site can be written as

$$\mathbf{G} = \left[M\omega^2 \mathbf{I} - \sum_{i=1}^{4} \langle \mathbf{K}_i \rangle \right]^{-1} = \left[M\omega^2 - \frac{4}{3}(K_{\parallel} + 2K_{\perp}) \right]^{-1} \mathbf{I}, \quad (9)$$

where $\mathbf{I}$ is the 3×3 identity matrix and M is the Si (A) mass. The last step in (9) follows from the tetrahedral symmetry of bonds i.

The Green's function at the oxygen site ($\mathbf{g}$) is easily obtained in terms of the calculated quantities [see Eqs. (18)–(23) in BGM] and the VDOS $\rho(\omega)$ of the glass per SiO_2 unit is

$$\rho(\omega) = \frac{-2\omega}{3\pi} \mathrm{Im}(M \,\mathrm{Tr}\mathbf{G} + 2m \,\mathrm{Tr}\mathbf{g}), \quad (10)$$

where m is the oxygen mass.

The Raman response of the glass is calculated as in BGM using a bond polarizability model, in which the polarized part of the spectrum is shown to be proportional to the symmetric stretching of the bonds at the nontetrahedral (oxygen) sites.

This Bethe lattice model represents the Raman response of the host network quite satisfactorily, as shown in Fig. 5. The experimentally measured reduced Raman spectra of v-SiO_2 are shown in Fig. 5(a), and the derived polarized portion $I^{\mathrm{PP}}_{\mathrm{Red}} \equiv (\mathrm{HH}\text{-}\frac{4}{3}\mathrm{HV})$ in Fig. 5(b). $I^{\mathrm{PP}}_{\mathrm{Red}}$ shows that the dominant Raman line (R) at about 450 cm^{-1}, as well as D_1 and D_2, are highly polarized lines which must be due to symmetric stretching of Si-O bonds along the bisectors of the Si-O-Si (θ) angles in the glass.

The polarized portion of the Raman response calculated with the theory just described is shown in Fig. 5(c), using the best fit parameters of BGM, given in the figure. Comparison with Fig. 5(b) is quite satisfactory. The theory produces a strong broad peak at about 450 cm^{-1} and a weaker less broad peak at about 800 cm^{-1}, in accordance with experiment. The CRN–Bethe-lattice theory does not yet contain regular rings.

The best fit force constants are in reasonable agreement with other calculations,[35] but the angle $\theta = 154°$ is somewhat larger than the most probable value $\theta = 144°$, deduced from x-ray diffraction experiments.[37] This discrepancy is not important since as was shown in BGM, variation of θ most strongly affects the position of the band near 800 cm^{-1}, far from the bands of our greatest interest (R, D_1, D_2). In fact, θ was chosen to best fit the position of this 800 cm^{-1} band.

B. Planar 3-ring dynamics

1. *Formulation in the cluster–Bethe-lattice approximation*

The results for $\langle \mathbf{K}_1 \rangle$ can be used to formulate the dynamics of a planar 3-ring in the cluster–Bethe-lattice approximation. The geometry is depicted in Fig. 4. We take ϕ to be tetrahedral ($\phi = \phi_T = 109.5°$) in the ring as it was in the CRN Bethe lattice. Following the energy minimization arguments in Sec. I C, we take the ring to be planar and hence $\theta = \theta_3 = 130.5°$. All six atoms are in the y-z plane of the paper, and each pair of bonds from a Si atom to the network is in a plane perpendicular to the paper, one bond up and one down. All angles at the Si atoms are tetrahedral. (We sometimes refer to these outgoing bonds as "ears" of the ring.)

Because there are six atoms in the ring, the symmetrical dynamical matrix is 18×18 and the Green's function for the ring can be written as

$$\mathbf{G}^{-1} = \mathbf{A}, \quad (11)$$

where $\mathbf{A}$ is a symmetric matrix, with

$$\mathbf{A}_{11} = M\omega^2 \mathbf{I} - \mathbf{\Sigma},$$
$$\mathbf{A}_{22} = M\omega^2 \mathbf{I} - \mathbf{R}^T \mathbf{\Sigma} \mathbf{R},$$
$$\mathbf{A}_{33} = M\omega^2 \mathbf{I} - \mathbf{R} \mathbf{\Sigma} \mathbf{R}^T,$$
$$\mathbf{A}_{44} = M\omega^2 \mathbf{I} + \mathbf{D}_4 + \mathbf{R}^T \mathbf{D}_6 \mathbf{R},$$

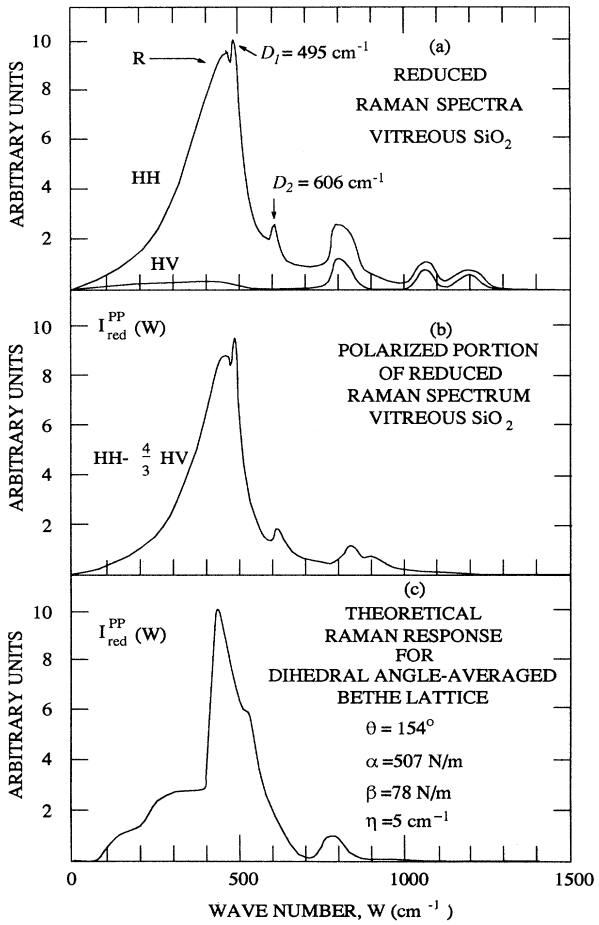

FIG. 5. A comparison of the experimentally measured reduced Raman spectra (a) of v-SiO_2 and the derived polarized portion [PP] (b) with the theoretical PP response (c) calculated for a Bethe lattice model with the parameters given. The Bethe lattice does not account for the sharp Raman lines D_1 and D_2 seen in experiment.

$$\mathbf{A}_{55} = M\omega^2\mathbf{I} + \mathbf{R}^T\mathbf{D}_4\mathbf{R} + \mathbf{R}\mathbf{D}_6\mathbf{R}^T,$$
$$\mathbf{A}_{66} = M\omega^2\mathbf{I} + \mathbf{R}\mathbf{D}_4\mathbf{R}^T + \mathbf{D}_6,$$
$$\mathbf{A}_{14} = -\mathbf{D}_4,$$
$$\mathbf{A}_{16} = -\mathbf{D}_6,$$
$$\mathbf{A}_{24} = -\mathbf{R}^T\mathbf{D}_6\mathbf{R},$$
$$\mathbf{A}_{25} = -\mathbf{R}^T\mathbf{D}_4\mathbf{R},$$
$$\mathbf{A}_{35} = -\mathbf{R}\mathbf{D}_6\mathbf{R}^T,$$
$$\mathbf{A}_{36} = -\mathbf{R}\mathbf{D}_4\mathbf{R}^T,$$

and all unspecified $\mathbf{A}_{ij}$ are $\mathbf{0}$. Each $\mathbf{A}_{ij}$ is a symmetric 3×3 matrix, and the rows and columns in $\mathbf{A}$ correspond to atoms numbered as in Fig. 4. The interactions between atom 1 and atoms 4 and 6 are given by

$$\mathbf{D}_4 = \begin{pmatrix} -\beta' & 0 & 0 \\ 0 & -\frac{1}{3}(2\alpha'+\beta') & -\frac{\sqrt{2}}{3}(\alpha'-\beta') \\ 0 & -\frac{\sqrt{2}}{3}(\alpha'-\beta') & -\frac{1}{3}(\alpha'+2\beta') \end{pmatrix} \quad (12)$$

and

$$\mathbf{D}_6 = \begin{pmatrix} -\beta' & 0 & 0 \\ 0 & -\frac{1}{3}(2\alpha'+\beta') & \frac{\sqrt{2}}{3}(\alpha'-\beta') \\ 0 & \frac{\sqrt{2}}{3}(\alpha'-\beta') & -\frac{1}{3}(\alpha'+2\beta') \end{pmatrix}, \quad (13)$$

where the primes ($'$) indicate force constants in the ring, generally assumed to be different than those in the CRN Bethe lattice (because angles θ are different). The matrix $\mathbf{R}$ in Eq. (11) is a rotation around the x axis by $2\pi/3$; it is clear that all interactions in the ring can be written in terms of $\mathbf{D}_4$ and $\mathbf{D}_6$ by using this rotation.

The quantity $\mathbf{\Sigma}$ represents the connection of the Si atom at 1 to the rest of the network through the two bonds in the x-z plane. Assuming that both bonds are satisfied by the CRN Bethe lattice, one has

$$\mathbf{\Sigma}_4 = \begin{pmatrix} -\frac{2}{3}(2K_\parallel + K_\perp) - 2\beta' & 0 & 0 \\ 0 & -2K_\perp - \frac{2}{3}(2\alpha'+\beta') & 0 \\ 0 & 0 & -\frac{2}{3}(K_\parallel + 2K_\perp) - \frac{2}{3}(\alpha'+\beta') \end{pmatrix}. \quad (14)$$

2. *Perfect decoupling responses of the 3-ring*

The matrix in Eq. (11) is readily inverted to give $\mathbf{G}$ and then the Raman response of the whole system is calculated. Some results are shown in Fig. 6.

Figure 6(a) shows the polarized portion of the Raman response of the ring when one uses the force constants of the Bethe lattice for those in the ring, i.e., for $\alpha' = \alpha$ and $\beta' = \beta$. The Raman response of the ring is seen to be very similar to that of the CRN Bethe lattice [compare with Fig. 5(c)]. According to this result, the ring breathing mode had a FWHM $\sim$ 100 cm^{-1}, far wider than the experimental value of $\sim$ 30 cm^{-1} for D_2 [see Fig. 5(a)]. The ring mode is broadened by the coupling of its motions to those of the CRN Bethe lattices.

According to the discussion in Sec. I E, perfect decoupling of the ring breathing mode occurs when Eq. (1) is satisfied, at a frequency given by Eq. (2). When we require that W_d = 606 cm^{-1}, the ring force constants are as given in Fig. 6(b). The Raman response of the ring is now a δ function at the frequency (606 cm^{-1}) of the decoupled breathing mode. The 10 cm^{-1} width shown in Fig. 6(b) is artificially produced by adding a small imaginary part ($\eta \sim 5$ cm^{-1}) to the frequency W. This avoids computational problems associated with peaks which are infinitely high and narrow. The ring force constants are now *different* than those used for the CRN Bethe lattice; however, in GBME it is pointed out that they vary in the expected directions with respect to the reduction of θ from 154° in the Bethe lattice to 130.5° in the ring.

The infrared (IR) activity of the ring in the Bethe lattice was estimated using the model developed by BGM for the CRN Bethe lattice. The result is shown in Fig. 6(c). There are weak broad responses from about 100 cm^{-1} to 1300 cm^{-1}, and two sharp responses at about

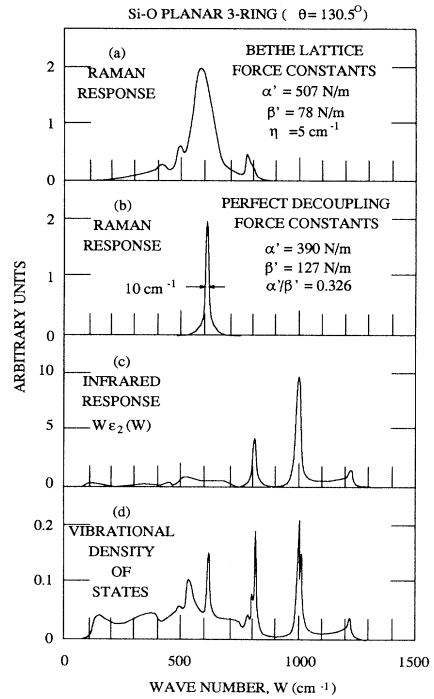

FIG. 6. Calculated vibrational responses of the planar 3-ring depicted in Fig. 4 with parameters appropriate for v-SiO_2. The PP Raman response in (a) is for ring force constants the same as those for the Bethe lattices representing the attached network. The oxygen breathing mode shown in (b) at 606 cm^{-1} is obtained for force constants in the ring as shown, satisfying the perfect decoupling condition, Eq. (1), and for Bethe lattice force constants as in (a). The infrared response (c) and the VDOS (d) of the ring are calculated for the same parameters as in (b).

800 cm^{-1} and 1000 cm^{-1}. No one has looked explicitly for these sharp lines in the infrared spectra of v-SiO_2, but the careful experiments of Gaskell *et al.*[45] do not reveal their presence, nor does the infrared dielectric function ϵ_2 reported by Galeener and Luckovsky.[10] This is most likely due to several factors: (1) In normal v-SiO_2 Galeener[28] has estimated that at most 1% of the oxygen atoms are in planar 3-rings, and so the IR lines would be weak; (2) in reality the lines would be broader than shown in Fig. 6(c), because their motions are *not* decoupled from the rest of the lattice; and (3) both lines would tend to be lost in the strong network response occurring at the same frequency. Figure 6(c) shows ring responses only, to which a much larger network response must be added.

Nevertheless, it would be interesting to measure high signal-to-noise IR spectra in special a-SiO_2 samples where the strength of D_2 has been greatly increased, as in porous Vycor[29] or partially desiccated sol-gel SiO_2.[30] One might then see some IR lines associated with the structure giving rise to D_2. Their positions should be predicted approximately as in Fig. 6(c).

The local vibrational density of states for the 3-ring is computed as the imaginary part of the trace of **G**, determined by Eq. (11). This is plotted in Fig. 6(d) for the perfect decoupling constant listed in Fig. 6(b). The ring shows modes over the full range of frequencies permitted to the Bethe lattice, although three of them are rather sharp because of the highly regular geometry of the ring. These three show up as the dominant Raman response of the ring (606 cm^{-1}) and the dominant IR responses ($\sim$ 800 cm^{-1} and $\sim$ 1000 cm^{-1}).

Because some modes are narrow and therefore fairly well decoupled from the network, one could gain some insight into those modes by considering the vibrations of a 6-atom Si_3O_3 "molecule." The normal modes of this molecule transform as the irreducible representations of the point group D_{3h}. They are $2A_1' + A_2' + A_2'' + 3E' + E''$ (a total of 12, because A modes are not degenerate while E modes have double degeneracy). The perfectly decoupled breathing mode has A_1' symmetry and the two sharp infrared modes are E'.

3. *Imperfect decoupling of 3-rings*

The perfect decoupling condition in Eq. (1) requires a precise relationship between forces constants (α', β') and ring angles (θ, ϕ). While the 3-ring angles are unchanged in various AX_2 tetrahedral glasses, the force constants will vary greatly. There is therefore no reason for Eq. (1) to be satisfied exactly in any glass, and we must test the assumption that approximate decoupling is adequate to explain the data.

We utilize the full cluster–Bethe-lattice model with "best fit" α and β for the Bethe lattice. The Raman response of the ring is calculated for various β'/α', with α' adjusted to keep the peak at 606 cm^{-1}.

Figure 7(a) shows the 3-ring linewidth versus β'/α', and Fig. 7(b) shows the corresponding values of α' and β'. We conclude that β'/α' can vary between 0.20 and 0.56 and still predict a D_2 linewidth below the observed value (40 − 10 = 30 cm^{-1}). Since acceptable β'/α' vary by nearly a factor of 3, the decoupling condition is not very stringent, and it is reasonable to believe that chemical bonding provided a ratio of central and noncentral forces that allow for adequate decoupling of the 3-ring breathing mode in v-SiO_2.

C. Regular 4-ring dynamics

As described in Sec. I, the Raman line D_1 at 495 cm^{-1} has been assigned to the breathing motion of a regular but puckered 4-ring. This is based on the appropriateness of the observed energy of formation,[35] the reported vibrational frequencies of the ring molecules such as octamethyltetracyclosiloxane[46] and by substantial elimination of other possibilities.[27] The assignment assumes decoupling of the mode from the network. To further test this hypothesis we must model the dynamics of a regular 4-ring and determine if the observed narrow linewidth (FWHM= 20 cm^{-1}) is consistent with the expected dynamics.

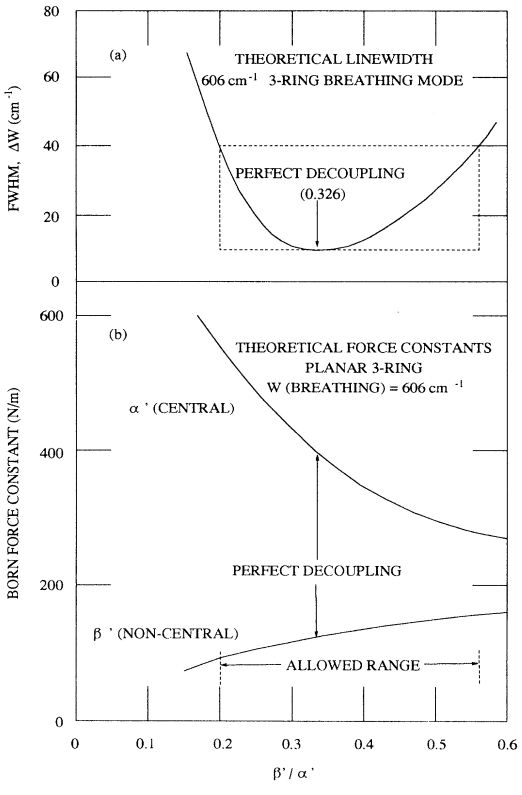

FIG. 7. The calculated full width at half maximum (FWHM) Raman linewidth (a) for the Bethe-lattice-terminated planar 3-ring in v-SiO_2, showing that the decoupling condition need not be perfect. That is, ΔW is less than or equal to observation (40 − 10 = 30 cm^{-1}) over a large range of ring force constant ratios ($0.2 \leq \beta'/\alpha' \leq 0.56$). The corresponding force constants (b) are within a reasonable range of those for the Bethe lattice, given in Fig. 6(a).

1. *Regular conformations of a 4-ring*

In order for the ring to have a single breathing-mode frequency we will assume that all Si-O-Si angles θ are the same in the ring, and of course that all O-Si-O angles ϕ are tetrahedral.

At the top of Fig. 8 are shown the eight atoms in a 4-ring, labeled as Si and O. Figure 8(a) shows all eight atoms in a single plane. Figure 8(b) shows a regular conformation in which the four Si atoms remain in the plane (○) while the two opposite O atoms are raised above the plane (+) and two others are lowered below the plane (−). With the help of the diagrams or a ball and stick model, the reader can verify that all eight conformations (a)–(h) in Fig. 8 are regular, in the sense defined above.

Of these eight configurations only two are capable of perfect decoupling of the breathing mode. If the Si atoms are to sit still (perfect decoupling) and the O atoms are to move along the bisector of θ, then only the planar ring (a) and the oxygen boat (b) can have central ($\vec{F}$) and noncentral ($\vec{G}$) forces antiparallel, in the manner illustrated in Fig. 4. Since perfect decoupling may not be required, as it was not required for the 3-ring, it is possible that some other conformations should be considered as candidates for D_1; however, we will first limit ourselves to those rings clearly capable of perfect decoupling.

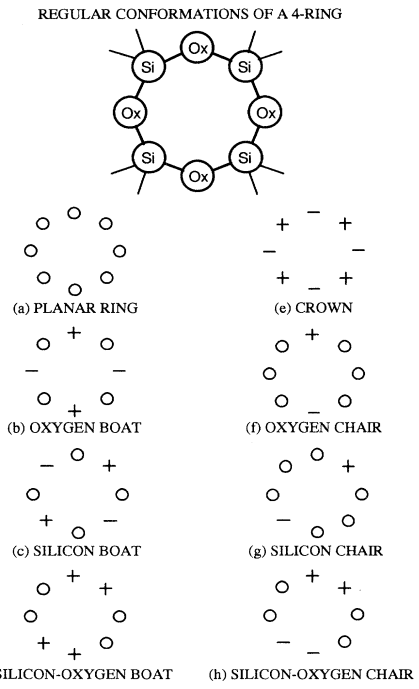

FIG. 8. A schematic representation of the eight regular conformations (a)–(h) of a 4-ring in a AX_2 tetrahedral glass such as v-SiO_2. The relative position of Si and O atoms around the ring is a common "median" plane, and so their height relative to the plane is denoted zero (○) in panel (a). In other panels, plus (+) denotes a position above the plane and minus (−) a position below the plane. Thus in the crown configuration (e) all four Si atoms are an equal distance above the median plane and all four O atoms are below by the same amount. In each of these conformations, all angles θ have a common value, and all $\phi = \phi_T$.

As discussed in Sec. I C, energy minimization suggests that the lowest energy 4-rings in a glass will be puckered, not planar. Also, *molecules* containing Si-O 4-rings tend to be puckered.[46] We thus eliminate the planar 4-ring from further discussion, and concentrate on the dynamics of the oxygen boat 4-ring.

2. *Formulation of oxygen boat 4-ring dynamics*

Figure 9 depicts an oxygen boat 4-ring. The oxygen bridges are tilted respect to the plane of the paper by a rotation about the dashed line joining two neighboring Si atoms, shown in the plan view of Fig. 9. This puckering of the ring is accomplished while keeping all angles ϕ tetrahedral and all angles θ the same. It is clear that θ for the puckered ring is less than θ for the planar ring. The angle of rotation γ about the line joining two Si atoms is related to θ and ϕ according to

$$\cos\gamma = \frac{\sin(\theta/2) - \sqrt{2}\cos(\phi/2)}{\cos(\theta/2)},$$

and using $\phi = \phi_T$ this becomes

$$\cos\gamma = \left[\sin(\theta/2) - \sqrt{2/3}\right] / \cos(\theta/2). \tag{15}$$

The angle γ is useful for visualizing the geometry of the puckered ring; however, for the purpose of our calculations, it is more convenient to produce the puckered ring by a set of rotations of the four SiO_4 tetrahedra comprising the ring. Consider a tetrahedron in the lower corner of the plan view in Fig. 9, and imagine two of the oxygen atoms to be in the plane of the figure, arranged symmetrically about the axis from that Si atom to the

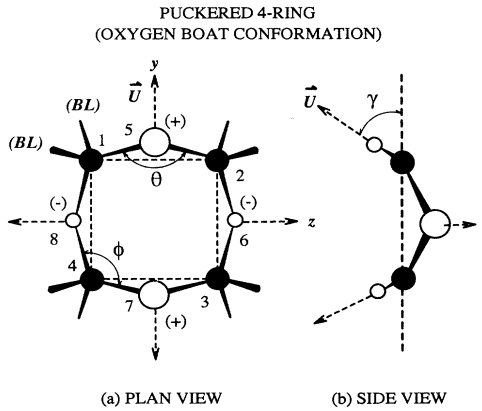

FIG. 9. The geometry of a regular puckered 4-ring in the oxygen boat configuration of Fig. 8(b). The atoms are numbered 1–8 as shown in (a). All Si atoms (solid) are in the y-z plane, while alternating oxygen atoms (open) are above (+) and below (−) the plane, by equal distances. For equal bond lengths and for all $\phi = \phi_T$ it is clear that all four angles θ have the same value; hence the ring is *regular*. The extent of nonplanarity (or "puckering") is readily perceived from the value of the angle γ depicted in (b).

opposing Si atom in the upper right corner. Define a rotation $\mathbf{S}(\psi)$ about the latter axis, where ψ is the angle of rotation which just brings the two oxygen atoms to their positions in the puckered ring actually shown in the plan view. A similar rotation $\mathbf{S}(\psi)$ of the tetrahedron at the opposite corner will completely reproduce the puckered ring. The necessary rotation ψ is related to θ by

$$\cos\psi = \sqrt{3}\sin\frac{\theta}{2} - \frac{1}{\sqrt{2}}\,. \tag{16}$$

The advantage of this construction is that it can be expressed as a rotation matrix and it clearly preserves ϕ at the tetrahedral value.

The formulation of 4-ring dynamics proceeds as in the 3-ring case, except that the eight atoms in the ring produce a 24×24 matrix equivalent to Eq. (11) with 3×3 blocks corresponding to each pair of interacting sites. Two rotation matrices are now required: $\mathbf{S}(\psi)$, just defined, and $\mathbf{R}$, which is a rotation of $\pi/4$ about an axis perpendicular to the plane and passing through the center of the ring. Note that all the Si atoms are in a plane and that the positions of O atoms are reproduced by rotations of $\mathbf{S}(\pm\psi)$ in alternate tetrahedral units.

The Green's function of the oxygen boat 4-ring becomes

$$\mathbf{G}^{-1} = \mathbf{B}, \tag{17}$$

where $\mathbf{B}$ is a symmetric matrix, and

$$\begin{aligned}
&\mathbf{B}_{11} = M\omega^2\mathbf{I} - \mathbf{S}^T\mathbf{R}\boldsymbol{\Sigma}\mathbf{R}^T\mathbf{S}\,, && \mathbf{B}_{15} = -\mathbf{S}^T\mathbf{R}\mathbf{D}_4\mathbf{R}^T\mathbf{S}\,, && \mathbf{B}_{18} = -\mathbf{S}^T\mathbf{R}\mathbf{D}_6\mathbf{R}^T\mathbf{S}\,,\\
&\mathbf{B}_{22} = M\omega^2\mathbf{I} - \mathbf{S}\mathbf{R}^2\boldsymbol{\Sigma}\mathbf{R}^{T2}\mathbf{S}^2\,, && \mathbf{B}_{25} = -\mathbf{S}\mathbf{R}^2\mathbf{D}_6\mathbf{R}^{T2}\mathbf{S}^T\,, && \mathbf{B}_{26} = -\mathbf{S}\mathbf{R}^2\mathbf{D}_4\mathbf{R}^{T2}\mathbf{S}^T\,,\\
&\mathbf{B}_{33} = M\omega^2\mathbf{I} - \mathbf{S}^T\mathbf{R}^{T2}\boldsymbol{\Sigma}\mathbf{R}^2\mathbf{S}\,, && \mathbf{B}_{36} = -\mathbf{S}^T\mathbf{R}^{T2}\mathbf{D}_6\mathbf{R}^2\mathbf{S}\,, && \mathbf{B}_{37} = -\mathbf{S}^T\mathbf{R}^{T2}\mathbf{D}_4\mathbf{R}^2\mathbf{S}\,,\\
&\mathbf{B}_{44} = M\omega^2\mathbf{I} - \mathbf{S}\mathbf{R}^T\boldsymbol{\Sigma}\mathbf{R}\mathbf{S}^T\,, && \mathbf{B}_{47} = -\mathbf{S}\mathbf{R}^T\mathbf{D}_6\mathbf{R}\mathbf{S}^T\,, && \mathbf{B}_{48} = -\mathbf{S}\mathbf{R}^T\mathbf{D}_4\mathbf{R}\mathbf{S}^T\,,
\end{aligned}$$

$$\begin{aligned}
&\mathbf{B}_{55} = m\omega^2\mathbf{I} + \mathbf{S}^T\mathbf{R}\mathbf{D}_4\mathbf{R}^T\mathbf{S} + \mathbf{S}\mathbf{R}^2\mathbf{D}_6\mathbf{R}^{T2}\mathbf{S}^T, && \mathbf{B}_{66} = m\omega^2\mathbf{I} + \mathbf{S}\mathbf{R}^2\mathbf{D}_4\mathbf{R}^{T2}\mathbf{S}^T + \mathbf{S}^T\mathbf{R}^{T2}\mathbf{D}_6\mathbf{R}\mathbf{S},\\
&\mathbf{B}_{77} = m\omega^2\mathbf{I} + \mathbf{S}^T\mathbf{R}^{T2}\mathbf{D}_4\mathbf{R}^2\mathbf{S} + \mathbf{S}\mathbf{R}^T\mathbf{D}_6\mathbf{R}\mathbf{S}^T, && \mathbf{B}_{88} = m\omega^2\mathbf{I} + \mathbf{S}\mathbf{R}^T\mathbf{D}_4\mathbf{R}\mathbf{S}^T + \mathbf{S}^T\mathbf{R}\mathbf{D}_6\mathbf{R}^T\mathbf{S}.
\end{aligned}$$

The 20 unspecified elements ($\mathbf{B}_{12}$, $\mathbf{B}_{13}$, etc.) are $\mathbf{0}$. Each $\mathbf{B}_{ij}$ is a symmetric 3×3 matrix and i and j refer to atoms labeled in Fig. 9.

3. *Perfect decoupling response of the oxygen boat 4-ring*

Inversion of $\mathbf{B}$ gives $\mathbf{G}$ and enables calculation of the Raman response. When the force constants in the ring are assumed identical to those in the Bethe lattice, one finds the response shown in Fig. 10(a), a fairly narrow peak at 460 cm^{-1}, whereas D_1 occurs at 495 cm^{-1}.

As before, we will assume that force constants in the ring can differ from those in the Bethe lattice, and we will invoke perfect decoupling. Following the procedure used for the planar rings, the perfect decoupling condition is found to be

$$\left(\frac{\beta'}{\alpha'}\right)_d = \frac{\cos(\phi/2)(1+\cos\theta)}{\sin(\phi/2)\cos\psi + \cos(\phi/2)\cos\theta} \tag{18}$$

or, in terms of γ,

$$\left(\frac{\beta'}{\alpha'}\right)_d = \left[1 + \frac{\cos\gamma}{\sqrt{2}\cos(\theta/2)\cos(\phi/2)}\right]^{-1}. \tag{19}$$

For $\phi = \phi_T$ and eliminating the rotation angles using Eqs. (15) and (16),

$$\left(\frac{\beta'}{\alpha'}\right)_d = \cot(\theta/2)\left[\frac{\cos(\theta/2)}{\sqrt{3/2} - \sin(\theta/2)}\right]. \tag{20}$$

Evaluating Eq. (20) for $\theta = 154°$ (the value used in the Bethe lattice) yields $(\beta'/\alpha')_d = 0.207$. When this is used in Eq. (2), and the frequency is set to 495 cm^{-1} (for D_1) one obtains the ring force constants and the decoupled Raman response shown in Fig. 10(b). As before, the expected δ function is broadened to 10 cm^{-1} by the addition of a fictitious imaginary part ($\eta = 5$ cm^{-1}) to all frequencies.

The infrared response for perfect decoupling of the Raman mode is shown in Fig. 10(c). The sharp line at about 820 cm^{-1} appears to be almost decoupled also. In fact this mode has an unrealistically high frequency because of a shortcoming of our Born force model. The mode largely consists of out-of-plane motions of the Si and O atoms in the ring, and it is clear that such motions should involve a different and smaller noncentral force constant than appropriate for in-plane motions. The difficulty is almost entirely for this special out-of-plane mode and it is discussed in detail elsewhere.[42]

The infrared mode at ~ 1250 cm^{-1} is also rather narrow, with a FWHM ~ 30 cm^{-1}. Nevertheless, it is coupled to the lattice as shown by the following facts. If one calculates the mode for rings that are uncoupled one gets $W_u = 1148$ cm^{-1}, so that the mode frequency is raised to 1205 cm^{-1} by the influence of coupling to the CRN. No evidence has been reported for weak but sharp IR mode at this frequency. Since there is strong IR absorption by the network at this frequency, we presume that either there are not enough 4-rings to be seen in infrared, or the mode in question is more coupled to the network than our calculation predicts and is therefore broader and weaker.

The local VDOS of the atoms in the ring is shown in Fig. 10(d), as obtained from the imaginary part of the mass weighted trace of $\mathbf{G}$ in Eq. (17). The modes of the ring resonate in the bands of the CRN Bethe lattice, as can be verified by comparison with Fig. 4 in BGM.

In Sec. I C we argued that some 4-rings relax completely to the minimum energy value of $\theta = \langle\theta\rangle$ and hence become regular. This energy "bottleneck" for regular-

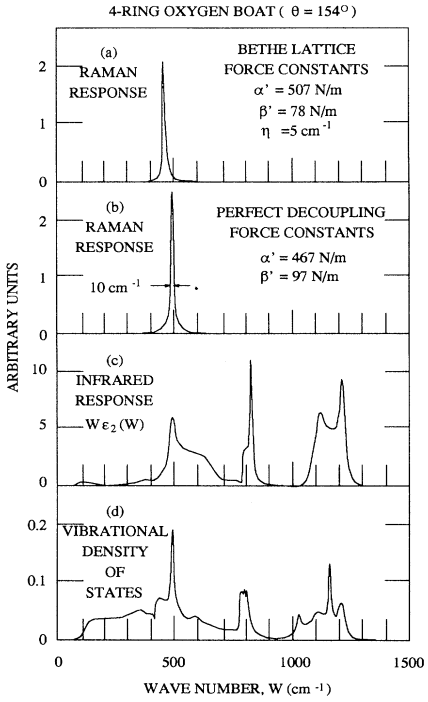

FIG. 10. Calculated vibrational responses of the regular oxygen boat 4-ring depicted in Fig. 9, with parameters appropriate for v-SiO_2. Here $\theta = 154°$, the best fit value for the Bethe-lattice representation of the CRN and therefore the minimum energy values for our dynamical calculations. The PP Raman response in (a) is for ring force constants the same as those of the best fit Bethe lattices representing the attached network. The oxygen breathing mode is moved to ~ 495 cm^{-1} in (b) for force constants in the ring as shown, satisfying the perfect decoupling condition, Eq. (1), and for the Bethe-lattice force constants as in (a). The infrared response (c) and the VDOS (d) of the ring are calculated for the same parameters as in (b).

ity of 4-rings does not seem as constricting on angle (θ) as does the kinetic bottleneck for regularity of 3-rings. Thus we must expect less regularity of θ in (nearly) regular 4-rings. Moreover, we have chosen $\theta = 154°$ so far simply because it provides a best fit to the broad lines in the spectra of v-SiO_2. Since x-ray diffraction shows $\langle\theta\rangle \simeq 144°$, we must admit the possibility of a different θ from that used. Therefore, we present Table I, showing ring force constants and ratios for several values of θ surrounding 154°, from $\theta = 160.5°$ (planar) to $\theta = 120°$. The values of α' and β' appear to be reasonable for $\theta \geq 146°$.

4. Imperfect decoupling of the oxygen boat 4-ring

As in the 3-ring case, we investigate the sensitivity of the width of the sharp Raman line to deviations from the perfect decoupling condition $\beta'/\alpha' = (\beta'/\alpha')_d$, given in Eqs. (18)–(20). In Fig. 11(a) the FWHM of the peak at 495 cm^{-1} is shown as a function of the force constant ratio. Comparison of this with Fig. 7(a) indicates that

TABLE I. The oxygen boat 4-ring force constants for perfect decoupling at $\omega(D_1) \equiv 495$ cm^{-1}, as a function of θ in the ring.

θ (deg)	α'/β'	α' (N/m)	β' (N/m)
160.53	0.121	790	95
160	0.128	748	96
158	0.153	628	96
154[a]	0.207	467	97
150	0.268	364	98
146	0.333	296	99
140	0.437	230	100
130	0.619	168	104
120	0.805	135	109

[a]Best fit.

the oxygen boat 4-ring is even less sensitive to deviations from perfect decoupling. We believe this fact explains that D_1 is sharper than D_2 in experiment.

The corresponding values of the constants in the ring are given in Fig. 11(b). Since the CRN–Bethe-lattice constants are $\alpha = 507$ N/m and $\beta = 78$ N/m, one has

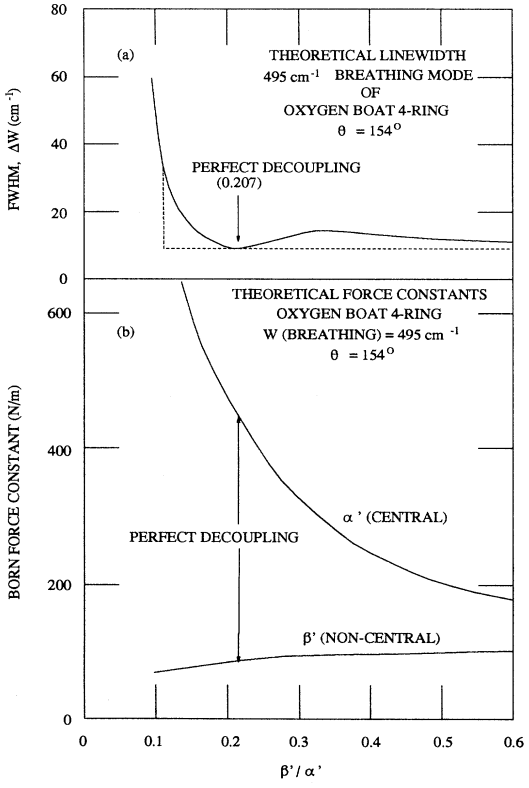

FIG. 11. The calculated full width at half maximum Raman linewidth (a) for the Bethe-lattice-terminated regular oxygen boat 4-ring in v-SiO_2, showing that the decoupling condition need not be perfect. That is, ΔW is less than or equal to observation ($30 - 10 = 20$ cm^{-1}) over a large range of ring force constant ratios β'/α' from 0.12 to something above 0.6. The corresponding force constants (b) are within a reasonable range of those for the best fit Bethe-lattice, given in Fig. 10(a).

to vary these only slightly to obtain perfect decoupling. For this reason, the peak in Fig. 10(a) is already quite narrow.

5. *Some results on the Si chair 4-ring*

We have found that the oxygen boat can be far from perfect decoupling and still give a sufficiently narrow D_1 line. Clearly this may also be true for regular rings that cannot perfectly decouple. We consider the example of the Si chair depicted in Fig. 8(g). This conformation is known to exist in the molecule hexamethylcyclotetrasiloxane[46] and may therefore be one of the low energy forms of regular 4-rings in the glass.

The dynamics of this ring is formulated in a manner completely analogous to that leading to Eq. (17). We omit the geometry and matrix algebra and merely present some results.

Figure 12(a) shows the Raman response of the silicon

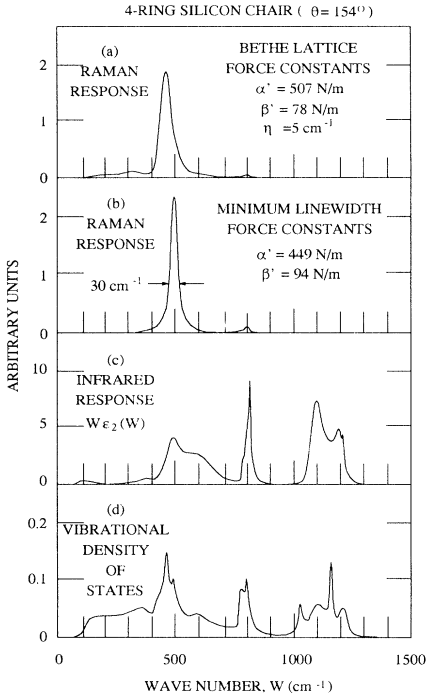

FIG. 12. Calculated vibrational responses of the regular silicon chair 4-ring depicted schematically in Fig. 8(g), with parameters appropriate for v-SiO_2. Here $\theta = 154°$, the best fit value for the Bethe-lattice representation of the CRN and therefore the minimum energy value for our dynamical calculations. The PP Raman response in (a) is for ring force constants the same as those of the best fit Bethe lattice representing the attached network. The oxygen breathing mode is moved to ~ 495 cm^{-1} in (b) for force constants in the ring as shown and for Bethe-lattice force constants as in (a). Perfect decoupling is not possible since $\vec{F}$ and $\vec{G}$ (cf. Fig. 4) are not antiparallel for this conformation. A computer search produced the force constants given, for minimum linewidths at $\omega \sim 495$ cm^{-1}. The infrared response (c) and the VDOS (d) of the ring are calculated for the same parameters as in (b).

chair 4-ring for ring force constants the same as those in the Bethe lattice. Although the frequency is almost correct at the D_1 line, the width is a bit too large. With a small change in force constants one can put the peak at 495 cm^{-1} and find a minimum width of $29 - 10 = 19$ cm^{-1}. Figure 12(b) is an example very near this condition, where the width is $30 - 10 = 20$ cm^{-1}.

The infrared response and VDOS for the silicon chair with the latter force constants are shown in Figs. 12(c) and 12(d), respectively. Notice the similarities with Figs. 9(c) and 9(d), which are for the oxygen boat.

We have determined that a sufficiently sharp line is obtained for a wide variation of the ratio β'/α'. In Table II is shown the calculated FWHM for $0.17 \leq \beta'/\alpha' \leq 0.24$, using $\theta = 154°$ and the α' and β' values (given) that keep the frequency at 495 cm^{-1}, and produce a *minimum* line width. That is, each entry in Table II represents a search over numerous values of α' and β', to find the pair that produces a *minimum* width. Each value should be reduced by 10 cm^{-1} for comparison with experimental reality. Acceptable linewidths are found for $0.18 \leq \beta'/\alpha' \leq 0.24$, and the range may be extended at this upper end.

The insensitivity of the linewidth variations in θ is shown in Table III, where the minimum width for various θ is reported, keeping the frequency at 495 cm^{-1}. The angle γ in the silicon chair is also given for easier visualization of the extent of puckering. It is defined as pictured in the side view of Fig. 9. The relation for the Si chair is

$$\cos\gamma = -(2\cos\theta/\sin\phi + 1). \tag{21}$$

Table III shows that one can pucker the ring out of the plane by as much as $\gamma = 50°$, attain $\theta = 152°$, and still have a sufficiently narrow line with reasonable values of α' and β'.

6. *Some results on the planar 4-ring*

For completeness we present one set of results for the planar 4-ring, showing that it too is relatively insensitive to perfect decoupling, but requires less reasonable force constants than the puckered ring. Table IV is for the planar ring ($\theta_4 = 160.5°$), where Eq. (1) predicts perfect

TABLE II. The insensitivity of the Raman linewidth (FWHM -10 cm^{-1}) of the oxygen breathing mode to the ratio β'/α' for a regular silicon chair 4-ring with $\theta = 154°$ (relaxed) and $\omega(D_1) \equiv 495$ cm^{-1}.

α' (N/m)	β' (N/m)	β'/α'	FWHM (cm^{-1})
525	89.2	0.17	34.0
502	90.5	0.18	31.5
482	91.5	0.19	31.0
463	92.5	0.20	31.0
449	94.2	0.21	28.0
427	94.0	0.22	29.0
414	95.1	0.23	30.0
400	95.8	0.24	30.0

TABLE III. The variation of the Raman linewidth (FWHM -10 cm^{-1}) of a regular silicon chair 4-ring versus θ for fixed $\omega(D_1) \equiv 495$ cm^{-1}. The extent of nonplanarity can be judged from the corresponding angle γ, defined in Fig. 9.

γ (deg)	α' (N/m)	β' (N/m)	β'/α'	θ (deg)	FWHM (cm^{-1})
0.0	790	95.5	0.121	160.5	10.0
38.5	554	94.2	0.17	156.1	27.5
51.4	370	94.2	0.255	151.6	31.5
66.5	205	96.2	0.47	142.2	35.0
77.3	119	102.5	0.86	130.5	38.0

decoupling at $(\beta'/\alpha')_d = 0.121$. The values of α and β that yield $\omega = 495$ cm^{-1} are shown, as is the resultant (FWHM -10 cm^{-1}), for various β'/α' that were calculated; however, the α' values are unreasonably large for $\beta'/\alpha' < 0.15$. Thus the completely acceptable range is approximately $0.15 < \beta'/\alpha' \leq 0.18$.

Comparison with Fig. 6(a) for the planar 3-ring indicates that the allowed range is much narrower for the planar 4-ring, and we expect it to be nonexistent for higher order rings. We thus conclude from dynamics alone that planar rings with $n \geq 4$ do not contribute to the sharp Raman lines (D_1 and D_2) because such rings are either unable to decouple sufficiently (for $n \geq 5$ the rings become involuted) or they require a very restricted and improbable range of values of β'/α' ($n = 4$).

On the other hand, we have shown that more than one regular conformation of a puckered 4-ring can sufficiently decouple over a wide range of β'/α' values. We thus have several arguments supporting the assignment of D_1 to a regular 4-ring: Regular 4-rings are expected to exist because of energy minimization arguments; and it will be easy for the value of β'/α' determined by chemistry to give sufficient decoupling, thereby satisfying the linewidth and isotopic substitution data.

D. Correlation of motions in the rings

Up to this point we have extracted information from the diagonal part of $\mathbf{G}$ [cf. Eqs. (11) and (17)] in order to get the local VDOS, and we have used the nondiagonal elements to calculate the Raman and infrared responses, using models presented in BGME. We will now gain some direct insight into the atomic motions involved by extracting information from the imaginary part of the nondiagonal elements of $\mathbf{G}$ in terms of the eigenvectors $|\, n\rangle$ of the Hamiltonian:

$$\mathbf{G}(E) = \sum_n \frac{|\, n\rangle\langle n\,|}{E - E_n}. \tag{22}$$

It then follows that

$$\begin{aligned} \mathrm{Im}\,[\mathrm{Tr}\mathbf{G}(E)] &= \mathrm{Im}\sum_{n'}\langle n' \mid \mathbf{G}(E) \mid n'\rangle \qquad (23)\\ &= \sum_{n'} \mathrm{Im}\left(\frac{1}{E - E_{n'}}\right) \\ &= -\pi \sum_{n'} \delta(E - E_{n'}) \\ &= -\pi\rho(E). \qquad (24) \end{aligned}$$

Now, any vector $|\, i\rangle$ of the system can be written as

$$|\, i\rangle = \sum_n C_{ni}\,|\, n\rangle, \tag{25}$$

so that

$$\begin{aligned} \langle i \mid \mathbf{G}(E) \mid j\rangle &= \sum_n \sum_m \sum_{m'} \frac{C^*_{im} C_{m'j} \langle m \mid n\rangle\langle n \mid m'\rangle}{E - E_n} \\ &= \sum_n \frac{C^*_{in} C_{nj}}{E - E_n}, \qquad (26) \end{aligned}$$

where we have used $\langle m \mid n\rangle = \delta_{mn}$. Thus, the imaginary part is proportional to the product of the coefficients of the vectors of every normal mode.

To understand this better, consider a normal mode at a particular frequency ω_0, whose basis vectors are the actual displacements of two atoms, say, a Si and a neighbor O in a ring. Then $\mathrm{Im}G^{xy}_{\mathrm{SiO}}$ is proportional to the coefficient of the oxygen motion in the y direction, and the coefficient of the silicon atom motion in the x direction, for the given normal mode. If $\mathrm{Im}G^{xy}_{\mathrm{SiO}}$ is very small, it means that when one moves the Si atom along x at frequency ω_0, the y motion of the O atom is unaffected; their motion is *uncorrelated*. If $\mathrm{Im}G^{xy}_{\mathrm{SiO}}$ is large and positive, the two atoms move in phase: Si motion along positive x is accompanied by O motion along positive y. Large negative $\mathrm{Im}G^{xy}_{\mathrm{SiO}}$ means the two motions are correlated, but out of phase.

Consider now the correlations of atomic motions within a planar 3-ring whose six external bonds are connected to the Bethe lattices having the same α and β as in the ring, and satisfying the perfect decoupling condition Eq. (1). In Fig. 13(a) we have plotted the imaginary part of

TABLE IV. The insensitivity of the Raman linewidth (FWHM -10 cm^{-1}) of a planar 4-ring to β'/α', for perfect decoupling at $\omega(D_1) \equiv 495$ cm^{-1}.

α' (N/m)	β' (N/m)	β'/α'	FWHM (cm^{-1})
1329	79.7	0.06	21
995	89.6	0.09	18
790	95.5	0.121	10
662	99.4	0.15	15
568	102.2	0.18	31

the trace of the 3×3 block corresponding to row 4 and column 5 of $\mathbf{G}$ in Eq. (11): This measures the correlation between two oxygen atoms in the ring (cf. Fig. 4). At low frequencies the correlation is positive and large, as it should be for the acoustic modes where the long wavelength means that the atoms follow each other in phase. At about 400 cm^{-1}, the correlation becomes negative, showing a deep peak at 606 cm^{-1}, the perfectly decoupled oxygen breathing mode of the planar 3-ring. Observe in Fig. 4 that in the breathing mode the xx and the yy correlations are zero, but the zz one is negative because the angle of the two oxygen displacements (bisecting θ) is greater than $\pi/4$.

That there is no Si motion in this mode is verified in Figs. 13(b) and 13(c), according to which there is no Si-O or Si-Si correlation at 606 cm^{-1}. At the infrared active frequencies, approximately 800 cm^{-1} and 1000 cm^{-1}, Fig. 13(b) shows strong negative correlation peaks, meaning that there is Si-O bond stretching. (These two infrared frequencies are related to ω_3 and ω_4 in central force analyses of the vibrations of an AX_2 tetrahedral network.[8])

Figure 14 shows the correlations of similarly defined motions in a regular oxygen boat 4-ring, for the parameters used in the perfect decoupling calculations shown in Fig. 10. At about 495 cm^{-1} one sees the large negative O-O correlation of the perfect decoupling oxygen breathing mode, as well as the zero Si-O and Si-Si correlations.

Figure 15 depicts the calculated correlations for a regular silicon chair 4-ring for the parameters used in the minimum linewidth calculations of Fig. 12. The correlations are very similar to those in Fig. 14 for the oxygen boat 4-ring. One expected difference is that at the frequency of the large, negative peak in O-O correlations (breathing mode) the silicon chair shows nonzero Si-Si correlation, evidence that the breathing mode is not perfectly decoupled.

We note that these 4-ring correlations show significant differences from the 3-ring correlations of Fig. 13, especially at high frequencies. This can be viewed as due to

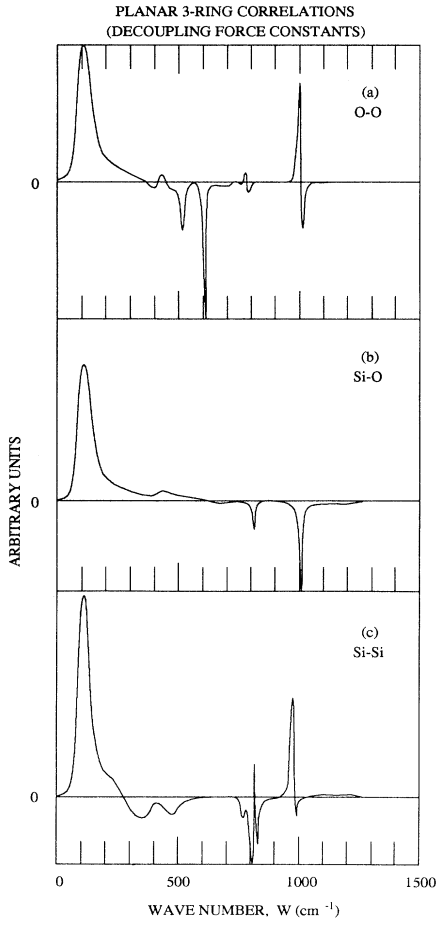

FIG. 13. Correlations of O-O motions (a), Si-O motions (b), and Si-Si motions (c) in the planar 3-ring for v-SiO_2. Positive values represent in-phase correlated motion of *neighboring* atoms in the ring, of the designated species, while negative values represent out-of-phase correlated motion. Values near zero indicate "uncorrelated" motion. For details see the text. Parameters are as in Fig. 6(b).

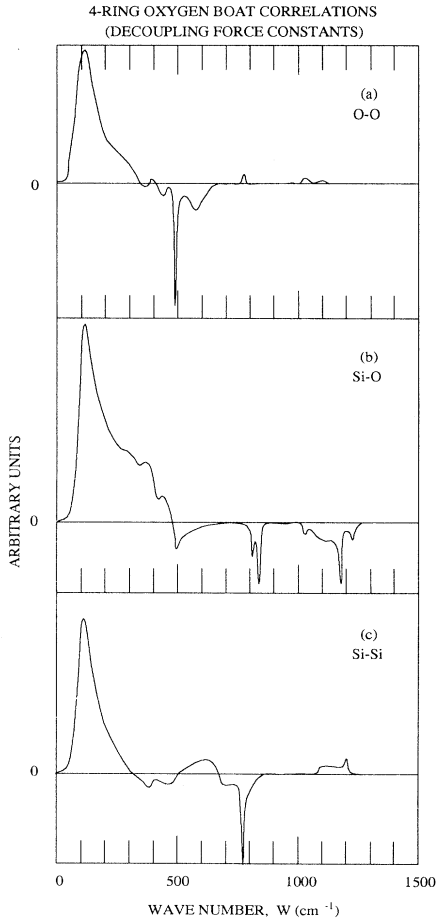

FIG. 14. Correlations of O-O motions (a), Si-O motions (b), and Si-Si motions (c) in the regular oxygen boat 4-ring, with perfect decoupling parameters given in Fig. 10(b). The meaning of large positive or negative correlations is as stated under Fig. 13 and in the text.

the difference in angle between two consecutive Si-O-Si units in the rings. For example, the infrared active mode at $\sim 1000\ \mathrm{cm}^{-1}$ in the planar 3-ring shows a large negative O-O correlation; however, the corresponding band in the 4-rings shows a very small positive O-O correlation, because neighboring Si-O-Si units are rotated by $\sim 90°$.

Since our model for infrared activity picks up the Si-O bond stretching motions, the large negative peaks in the Si-O correlations look very similar to the high frequency peaks in the appropriate infrared responses shown in Figs. 6(c), 10(c), and 12(c).

E. Application to v-GeO_2

Galeener[47] has previously applied the energy minimization argument of Sec. I to v-GeO_2, which is an AX_2 tetrahedral glass having $\langle\theta\rangle \simeq 133°$, according to diffraction studies.[48] Since a planar 3-ring of GeO_2 tetrahedra has $\theta = 130.5° \cong \langle\theta\rangle$, such a ring would have nearly zero energy stored in its Ge-O-Ge bridges. Accordingly, Galeener[38] has suggested that the v-GeO_2 contains larger numbers of nearly planar 3-rings than does v-SiO_2.

Figure 16(b) shows the polarized portion (HH-$\frac{4}{3}$HV) of the reduced Raman spectra of v-GeO_2.[9] The dominant Raman line R at 420 cm^{-1} has a FWHM of about 100 cm^{-1}, and is therefore substantially narrower than in v-SiO_2 [see Fig. 5(a)]. A large number of nearly planar 3-rings and perhaps regular 4-rings would produce a narrower distribution of θ in v-GeO_2 and thereby explain the observed narrowness of the dominant Raman line, as well as the observed narrowness of the Ge-Ge diffraction peak.[48] The 3-rings are expected to be less planar than in v-SiO_2 because we presume that it costs very little energy to have a bridge with θ differing only a few degrees from $\langle\theta\rangle = 133°$.

In this context, we present the computed Raman spectra for v-GeO_2 shown in Fig. 17. The upper panel (a) shows the Raman response of a Bethe lattice with $\theta = \langle\theta\rangle = 133°$, using α and β taken from BGM to provide a "best fit" to the position of the dominant Raman peak. The FWHM is about 70 cm^{-1}, whereas experiment shows $\sim 100\ \mathrm{cm}^{-1}$.

Figure 17(b) is for a planar 3-ring with the same α and β as in Fig. 17(a). The FWHM is narrower ($\sim 40\ \mathrm{cm}^{-1}$) and the peak is still very near 420 cm^{-1}. While the line

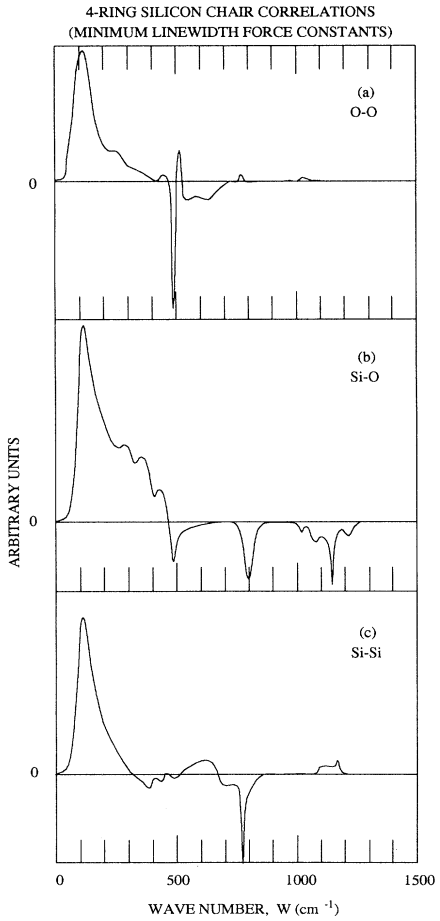

FIG. 15. Correlations of O-O motions (a), Si-O motions (b), and Si-Si motions (c) in the regular silicon chair 4-ring, with minimum linewidth parameters given in Fig. 12(b). The meaning of large positive or negative correlations is as stated under Fig. 13 and in the text.

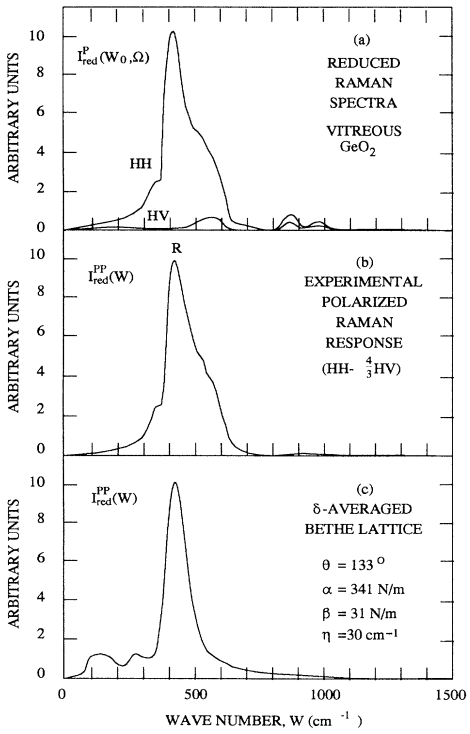

FIG. 16. A comparison of the experimentally measured reduced Raman spectra (a) of v-GeO_2 and the derived polarized portion (b), with the theoretical PP response (c) calculated for a Bethe lattice model with the parameters given. The Bethe-lattice parameters are chosen to fit the dominant Raman line position (420 cm^{-1}) and linewidth ($\sim 100\ \mathrm{cm}^{-1}$). Clearly (c) does not account for the experimental bumps at approximately 350, 520, and 600 cm^{-1}. We suggest that the first two are evidence for regular rings.

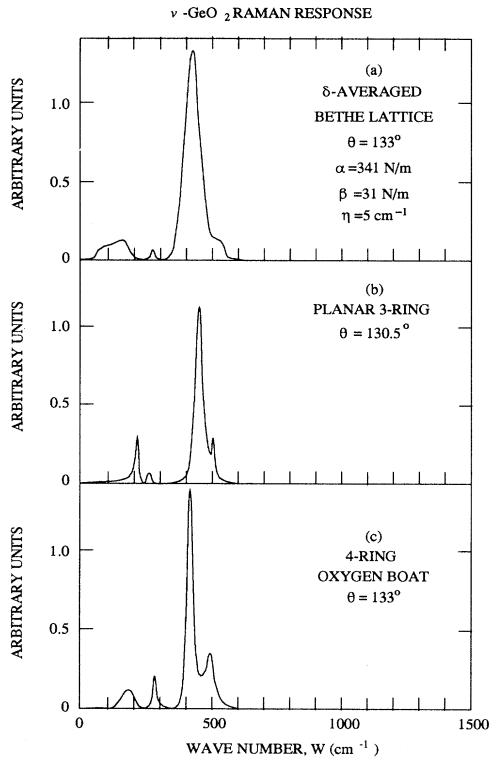

FIG. 17. Calculated PP Raman responses for v-GeO_2. The response of the best fit Bethe lattice is shown in (a), for parameters as in Fig. 16(c) (except that η has been reduced to 5 cm^{-1}, resulting in sharper features). The response of a planar 3-ring with ring force constants identical to those of the Bethe lattice in (a) is shown in (b). Force constants are expected to differ very little because $\theta_3 = 130.5° \simeq \langle\theta\rangle = 133°$. The ring response in (b) peaks at essentially the same W as the Bethe lattice in (a). The response of the relaxed regular oxygen boat 4-ring (c) is also computed for Bethe-lattice force constants in the ring, and also peaks at the same W as in (a). The sharp subsidiary peaks on either side of W_R in panels (b) and (c) are taken as origin(s) of experimental bumps at $\sim$ 350 and 520 cm^{-1} in Fig. 16(b).

is quite narrow, the oxygen breathing mode is clearly not perfectly decoupled from the Bethe lattice.

The Raman response of a regular oxygen boat 4-ring is shown in the lower panel, Fig. 17(c), calculated with α and β as above and with θ relaxed to $\langle\theta\rangle = 133°$. FWHM is now reduced to about 25 cm^{-1} and the peak is still very near 420 cm^{-1}.

Since there is negligible shift in R, the existence of the substantial numbers of planar 3-rings and regular 4-rings would lead to a *narrower* Raman line than expected from the Bethe lattice alone. If almost planar 3-rings dominate the structure, we would also expect so see fairly sharp subsidiary Raman peaks at about 220 cm^{-1} and 500 cm^{-1}. If regular oxygen boat 4-rings dominate, we would expect sharp, weak features at about 280 cm^{-1} and 520 cm^{-1}. Therefore, one or both of these kinds of rings may account for the small relatively narrow features seen in the data of Fig. 16 at about 350 cm^{-1} and 520 cm^{-1}.

We conclude that cluster–Bethe-lattice calculations of the Raman active vibrations of nearly planar 3-rings and regular 4-rings in v-GeO_2 are consistent with the assumption that large concentrations of such rings exist in the real glass. Such rings are able to account for the previously unexplained small features observed at both sides of R in Fig. 16.

III. CONCLUDING REMARKS

We have repeated an earlier argument that network energy is reduced when small rings of bonds become planar or regular in v-SiO_2. Thus there is an energy minimization rationale for small rings of bonds to be regular in an otherwise more disordered network.

Cluster–Bethe-lattice calculations of the dynamics of planar 3-rings are found to explain all known properties of the sharp Raman active line D_2, seen at 606 cm^{-1} in v-SiO_2. This requires that the rings be fairly regular, and that the ratio of their central to noncentral force constants be within a rather broad range which assures adequate decoupling of the oxygen breathing-mode motion from the rest of the network.

Similar calculations for regular oxygen boat and silicon chair 4-rings show that their vibrational properties are consistent with all known properties of the sharp Raman line D_1, seen at 495 cm^{-1} in v-SiO_2. Here, there is even more *leeway* available in the ratio of central to noncentral force constants and in the geometric perfection (regularity) of the 4-rings.

The resultant structural model involving small nearly regular rings of Si-O bonds explains many properties of the Raman active "defect" lines D_1 and D_2, including their frequencies, sharpness, Raman activity, Raman polarization, lack of companion Raman lines, energy of formation, isotope shifts (no Si motion), increase with neutron dose, and increase with internal surface area.

Since the planar 3-ring is under compressive strain, its presence may account microscopically for a significant proportion of compressive surface tension in v-SiO_2.

In recent molecular dynamics computer simulations[49] a study of n-fold rings reveals that about 1% of the total number of rings are 3-rings, although most of them were puckered in the crown configuration and no planar rings were found. This might be due to the strength of the three-body potentials used, particularly the ones involving O-Si-O bonds, which for some reason allow an exaggerated floppiness of the tetrahedral angle ϕ, which contradicts the observed rigidity of the SiO_4 tetrahedra. The mean value $\phi = 102°$ for the 3-rings in these computer simulations is unacceptable.

Since the planar 3-ring does not occur in any known crystalline form of v-SiO_2, Galeener[38] has suggested that its presence may significantly inhibit crystallization upon quenching. The concentration of planar 3-rings (strength of D_2) *increases* with fictive temperature T_F so that at the melting temperatures, there may be a very large concentration of these structural units which must first be broken in order to build any known crystalline form. As suggested elsewhere[38] the existence of large concentrations of these planar 3-rings may therefore be a key to un-

derstanding the strong glass-forming tendency of molten SiO_2 and the glass transition itself. *In general, the tendency to form a glass rather than a crystal may be due to specific elements of intermediate-range order in the melt, in the form of small regular rings of bonds, which do not exist topologically in any crystalline form of the substance.*

Similar arguments and cluster–Bethe-lattice calculations suggest that v-GeO_2 contains even more nearly planar 3-rings than does v-SiO_2. They also suggest that regular puckered 4-rings exist in significant numbers and account for "bumps" seen in the Raman spectra at ~ 350 and 520 cm^{-1}.

ACKNOWLEDGMENTS

The authors are grateful to several institutions and agencies for significant partial support of this work. They are The Xerox Palo Alto Research Center; the U.S. Navy Office of Naval Research, under Contracts Nos. N00014-80-C-0713 and N00014-91-J-1607 (G.B. Wright); the Cavendish Laboratory, University of Cambridge; Universidad Nacional Autónoma de México Project IN 101392; and the European Economic Community, Contract No. CI1-CT90-0864.

---

*Deceased.

†Present address: AT&T, Microelectrónica, España, Tres Cantos, Madrid, Spain.

[1]F.L. Galeener, Diffus. Defect Data **54-55**, 305 (1988).

[2]F.L. Galeener, Philos. Mag. Lett. B **51**, L1 (1985).

[3]R.L. Mozzi and B.E. Warren, J. Appl. Crystallogr. **2**, 164 (1969).

[4]F.L. Galeener, in *The Physics and Technology of Amorphous SiO_2*, edited by R.A.B. Devine (Plenum, New York, 1988), p. 1.

[5]R. Shucker and R.W. Gammon, Phys. Rev. Lett. **25**, 222 (1970).

[6]F.L. Galeener and P.N. Sen, Phys. Rev. B **17**, 1928 (1978).

[7]F.L. Galeener, Phys. Rev. B **19**, 4292 (1979).

[8]M.F. Thorpe and F.L. Galeener, Phys. Rev. B **22**, 3078 (1980).

[9]F.L. Galeener, A.J. Leadbetter, and M.W. Sringfellow, Phys. Rev. B **27**,1052 (1983).

[10]F.L. Galeener and G. Luckovsky, Phys. Rev. Lett. **37**, 1474 (1976).

[11]R.A. Barrio, F.L. Galeener, and E. Martínez, Phys. Rev. Lett. **52**, 1786 (1984).

[12]R.A. Barrio, F.L. Galeener, and E. Martínez, Phys. Rev. B **31**, 7779 (1985).

[13]R.H. Stolen, J.T. Krause, and C.R. Kurkjian, Discuss. Faraday Soc. **50**, 103 (1970).

[14]F.L. Galeener, J. Non-Cryst. Solids **40**, 527 (1980).

[15]J.C. Mikkelsen, Jr. and F.L. Galeener, J. Non-Cryst. Solids **37**, 71 (1980).

[16]F.L. Galeener, Kinam **4**, 83 (1982).

[17]A.E. Geissberger and F.L. Galeener, Phys. Rev. B **28**, 3266 (1983).

[18]F.L. Galeener and R.H. Geils, in *The Structure of Non-Crystalline Materials*, edited by P.H. Gaskell (Taylor & Francis, London, 1977), p. 223.

[19]J.C. Mikkelsen, Jr. and F.L. Galeener, Appl. Phys. Lett. **37**, 712 (1980); F.L. Galeener and J.C. Mikkelsen, Jr., Solid State Commun. **37**, 719 (1981).

[20]F.L. Galeener and J.C. Mikkelsen, Jr., Appl. Phys. Lett. **38**, 336 (1981); J.C. Mikkelsen, Jr. and F.L. Galeener, J. Mater. **10**, 631 (1981).

[21]F.L. Galeener and A.E. Geissberger, Phys. Rev. B **27**, 6199 (1983); J. Phys. (Paris) Colloq. **44**, C9-343 (1983).

[22]F.L. Galeener and J.C. Mikkelsen, Jr., Phys. Rev. B **23**, 5527 (1981).

[23]G.E. Walrafen, P.N. Krishnan, and S.W. Freiman, J. Appl. Phys. **52**, 2832 (1981).

[24]W. Primak, *The Compacted States of Vitreous Silica* (Gordon and Breach, New York, 1975).

[25]R.H. Stolen and G.E. Walrafen, J. Chem. Phys. **64**, 2623 (1976).

[26]G. Lucovsky, Philos. Mag. **39**, 515 (1979).

[27]A.R. Silin and P.J. Bray, Bull. Am. Phys. Soc. **26**, 218 (1981).

[28]F.L. Galeener, J. Non-Cryst. Solids **49**, 53 (1982).

[29]C.A. Murray and T.J. Greytak, J. Chem. Phys. **71**, 3555 (1979).

[30]A. Bertoluzza, C. Fagnano, M.A. Morelli, V. Gotardi, and M. Guglielmi, J. Non-Cryst. Solids **48**, 117 (1982).

[31]F.L. Galeener, in *The Structure of Non-Crystalline Materials*, edited by P.H. Gaskell, J.N. Parker, and E.A. Davis (Taylor & Francis, London, 1983), p. 337.

[32]C.J. Brinker, E.P. Roth, G.W. Scherer, and D.R. Tallant, J. Non-Cryst. Solids **71**, 171 (1985); C.J. Brinker, D.R. Tallant, E.P. Roth, and C.S. Ashley, *ibid.* **82**, 117 (1986); in *Defects in Glasses*, edited by F.L. Galeener, D.L. Griscom, and M.J. Weber, MRS Symposia Proceedings No. 61 (Materials Research Society, Pittsburgh, 1986), p. 387.

[33]F.L. Galeener, J. Phys. (Paris) Colloq. **42**, C6-24 (1981).

[34]R.M. Martin and F.L. Galeener, Phys. Rev. B **23**, 3071 (1981).

[35]F.L. Galeener, Solid State Commun. **44**, 1037 (1982).

[36]M.D. Newton and G.V. Gibbs, Phys. Chem. Miner. **6**, 221 (1980).

[37]P.G. Coombs, J.F. De Natale, R.S. Wortman, J.F. Shackelford, D.K. McElfresh, and P.J. Hood, Philos. Mag. B **51**, L39 (1985).

[38]F.L. Galeener, in *The Physics of Disordered Materials (a Festschrift for Sir Neville Mott)*, edited by D. Adler, H. Fritzsche, and S.R. Ovshinsky (Plenum, New York, 1985), p. 159.

[39]M. O'Keeffe and G.V. Gibbs, J. Chem. Phys. **81**, 876 (1984).

[40]F.L. Galeener, R.A. Barrio, E. Martínez, and R.J. Elliott, Phys. Rev. Lett. **53**, 2429 (1984).

[41]A.M. Stoneham, V.T.M. Torres, H.R. Schober, and P.M. Masri, Philos. Mag. A **58**, 93 (1988).

[42]R.A. Barrio, F.L. Castillo-Alvarado, and F.L. Galeener, Phys. Rev. B **44**, 7313 (1991).

[43]J.D. Joannopoulos and F. Yndurain, Phys. Rev. B **10**, 5164 (1974).

[44]F.L. Galeener and M.F. Thorpe, Phys. Rev. B **28**, 5802 (1983).

[45]P.H. Gaskell and D.W. Johnson, J. Non-Cryst. Solids **20**,

171 (1976); P.H. Gaskell and I.D. Tarrant, Philos. Mag. B **42**, 265 (1980).
[46]H. Steinfink, B. Post, and I. Fankuchen, Acta Crystallogr. **8**, 420 (1955).
[47]Reference 38; F.L. Galeener, in *Disorder in Condensed Matter Physics, A Volume in honor of Sir Roger Elliott*, edited by J. A. Blackman and J. Tagüeña, Oxford Science Publications (Oxford University Press, New York, 1991), p. 45.
[48]A.C. Wright, G. Etherington, J.A. Erwin-Desa, R.N. Sinclair, G.A.N. Connell, and J.C. Mikkelsen, Jr., J. Non-Cryst. Solids **49**, 63 (1982).
[49]J.P. Rino, I. Ebbsjö, R.K. Kalia, A. Nakano, and P. Vashishta, Phys. Rev. B **47**, 3053 (1993).